arXiv:1601.06082v1 [physics.atom-ph] 22 Jan 2016

Metrology with Atom Interferometry: Inertial Sensors from Laboratory to Field Applications

B Fang, I Dutta, P Gillot, D Savoie, J Lautier, B Cheng, C L Garrido Alzar, R Geiger, S Merlet, F Pereira Dos Santos and A Landragin

LNE-SYRTE, Observatoire de Paris, PSL Research University, CNRS, Sorbonne Universités, UPMC Univ. Paris 06, 61 avenue de l'Observatoire, 75014 Paris, France

E-mail: bess.fang@obspm.fr

Abstract. Developments in atom interferometry have led to atomic inertial sensors with extremely high sensitivity. Their performances are for the moment limited by the ground vibrations, the impact of which is exacerbated by the sequential operation, resulting in aliasing and dead time. We discuss several experiments performed at LNE-SYRTE in order to reduce these problems and achieve the intrinsic limit of atomic inertial sensors. These techniques have resulted in transportable and high-performance instruments that participate in gravity measurements, and pave the way to applications in inertial navigation.

1. Introduction

Since the advent of atom interferometers (AI) in 1990s ([1, 2], see also [3] and references therein), tremendous progress has been made to improve the performance as well as the transportability of inertial sensors based on AI. Today, these sensors have already been used in field applications such as geophysics measurements [4, 5], and promise to surpass other state-of-the-art technologies in inertial navigation [6]. Moreover, they are the prime candidates to explore some aspects of fundamental physics such as testing of Einstein Equivalence Principle [7], and detection of gravitational waves [8, 9].

The performance of AI-based inertial sensors is fundamentally limited by the noise in the measurement of the transition probability, i.e. the standard quantum projection noise (QPN) [10], or ideally the Heisenberg limit, between the two interferometric states. Vibration noise on the ground is however several orders of magnitude higher. The sequential operation of typical sensors exacerbates the problem by down aliasing higher-frequency noise, similar to the Dick effect in cold atomic clocks [11]. Dead time, during which the atoms are prepared or detected, results in loss of information of the inertial signal, preventing fast averaging of the vibration noise.

Different strategies have been proposed to overcome these difficulties. When a (nearly) stable quantity such as the gravitational acceleration $\vec{g}$ is measured in a stable environment (e.g. in a laboratory), one may average the noise out with longer measurements or perform active filtering [12, 13]. When transportability is required for measurements at different sites, the bulky active platform must be replaced by passive isolation systems and classical sensors that measure the aliasing effect as proposed in [10] and first demonstrated in [14]. The need to completely

eliminate dead time comes from applications in geophysics and inertial navigation, where the inertial signals would fluctuate in time and the environment is far from stable [15].

In this paper, we discuss several experiments performed in the LNE-SYRTE inertial sensor group to address the issues related to the vibration noise, aliasing and the dead time in order to explore the intrinsic limits of AI-based inertial sensors.

2. Inertial Sensors based on Atom Interferometry

We start with a brief description of common techniques used in cold-atom inertial sensors using alkali atoms and stimulated Raman transitions. These techniques are by no means unique, but are often practiced for their technological maturity. They have been proven reliable in high-performance instruments. However, the methods for reduction of vibration that we will describe in the subsequent sections can be extended to other schemes of atom interferometers.

Before the interferometric measurements start, an atomic source is loaded and laser cooled to reach sub-Doppler temperatures. These atoms are then launched or released into a free fall and enter the interferometric zone. A three-pulse atom interferometer is analogous to an optical Mach-Zehnder interferometer: the matter wave is split, deflected and recombined by counter-propagating Raman beams via two-photon transitions between two hyperfine states [2]. At the output of the interferometer, the population in each state is detected by fluorescence. This gives the transition probability P, which depends on the phase difference $\Delta\Phi$ experienced by the two arms of the interferometer, $P = \frac{1}{2}(1 + C\cos\Delta\Phi)$, where C is the contrast. Such a setup is illustrated in Figure 1 (a).

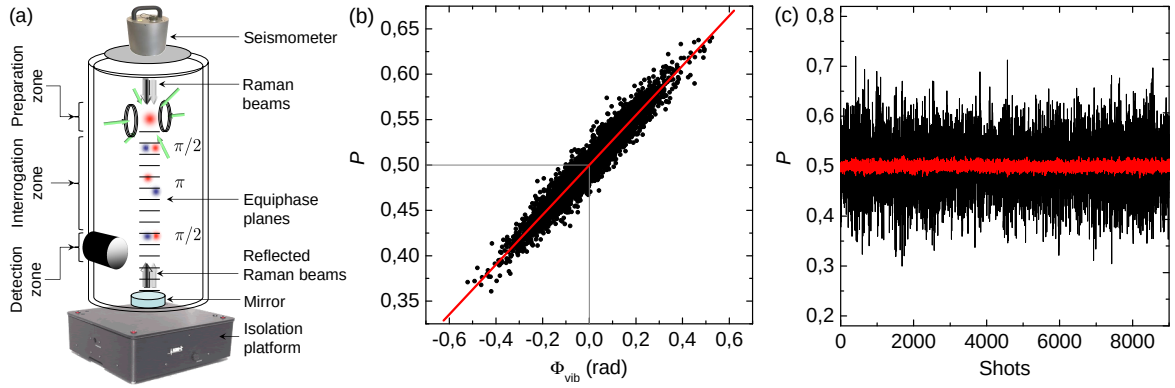

Figure 1. (a) Illustration of an atom gravimeter. It is mounted on a vibration isolation platform for passive isolation. A seismometer is rigidly fixed on the structure in order to record residual vibration noise of the retroreflection mirror. (b) Measured transition probability P vs the calculated vibration phase $\Phi_{\rm vib}$ (points). The linear fit (straight line) prompts a simple correction procedure by subtraction. (c) Transition probability P of a series of data points before (black) and after (red) correlation.

The interferometer phase $\Delta\Phi$ is the difference of the atomic phase accumulated along the two paths of the interferometer. It is given by $\Delta\Phi = \phi_1 - 2\phi_2 + \phi_3$, where ϕ_i denotes the phase difference of the Raman lasers at the center of the atomic wave packet during the ith interrogation pulse. Since the Raman beams are often retroreflected, the equiphase planes are defined by the mirror position, making the interferometer sensitive to the displacement in the direction of propagation of the beams [16]. We can thus write the interferometer phase as the sum of the desired signal and the noise (e.g. vibrations), $\Delta\Phi = \Phi_{\rm sig} + \Phi_{\rm noise}$.

3. Vibration Isolation and Correlation with Classical Sensors

We demonstrate here that passively isolating the atomic sensor from the environment and performing post correlations with classical sensors allow us to significantly improve the performance of an atom gravimeter and that of an atom gyroscope.

The LNE-SYRTE Cold Atom Gravimeter (CAG) uses free falling rubidium-87 atoms in a three-pulse ($\pi/2$-π-$\pi/2$) configuration. With the Raman beams in the vertical direction, the interferometer is sensitive to the gravitational acceleration $\vec{g}$, i.e. $\Phi_{\rm sig} = -\vec{k}_{\rm eff} \cdot \vec{g} T^2$, where $\vec{k}_{\rm eff}$ denotes the difference between the wave vectors of the two Raman lasers, and T is the time interval between successive Raman pulses.

We operate CAG with a cycling frequency of 3 Hz and a total interrogation time $2T = 160$ ms [17]. With about 10^6 atoms detected, the ground vibration introduces a noise 10^4 times the standard QPN limit. We passively isolate CAG with an anti-acoustic box and a vibration isolation platform, reducing the vibration noise by about a factor 100. We then acquire the vibration signal of the retroreflection mirror using a seismometer rigidly fixed on the the frame of CAG [see Fig. 1 (a)]. The fluctuating velocity of the mirror during the interrogation results in a shift of the interferometric phase $\Phi_{\rm noise} = \Phi_{\rm vib}$. This can be computed by integrating the acquired velocity with a weighting function that describes the response of the interferometer, known as the time transfer function (see [18] and references therein). Figure 1 (b) shows P versus $\Phi_{\rm vib}$. The linear relationship between these two quantities permits a simple correction procedure by subtraction [14]. The vibration rejection efficiency is about 10 in the present case [see Fig. 1 (c)], and has been measured to be up to 120 without passive isolation.

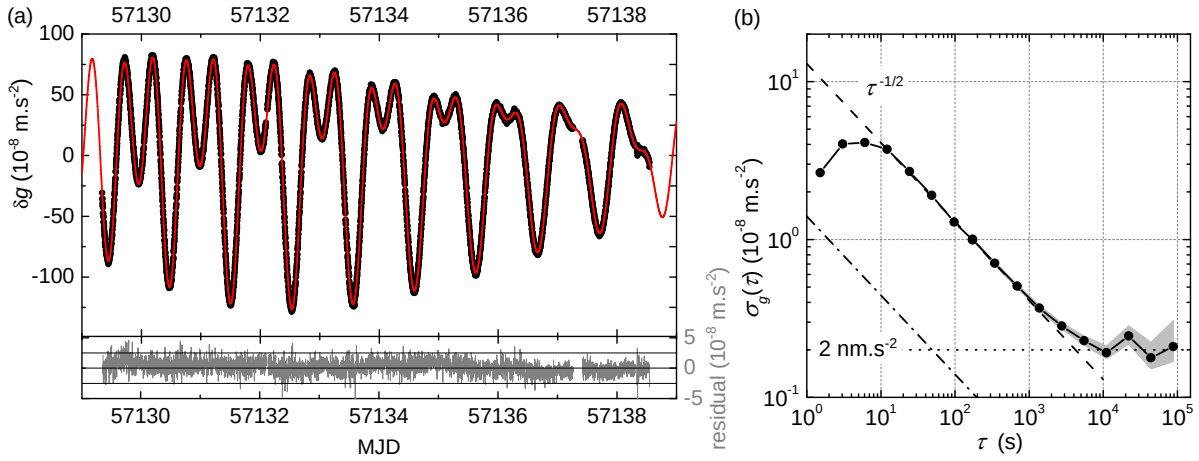

Figure 2. (a) Variation of g around its mean measured value as a function of days. Top: CAG measurement (points) averaged over 170 s and the tide model (line). Bottom: the residual (difference) between the measurement and the model. (b) ADEV of the CAG measurements corrected for the tides and local environmental effects. The shaded region indicates the uncertainty of the measurement, whereas the straight line gives the $\tau^{-1/2}$ scaling characteristic of averaging white frequency noise, where τ is the integration time. Similar trend lines will be given in subsequent figures with no further explanations. The dash-dotted line indicates the calculated QPN limit for typical parameters of 10^6 atoms, 40% contrast, and $T = 80$ ms.

We use CAG to record the temporal variation of gravity in our laboratory dedicated to gravity measurements [19]. Figure 2 (a) overlays the measured g and the tide model, showing an excellent agreement throughout the $\pm 10^{-7}$ relative variations around the mean value due to the lunisolar tide. The Allan standard deviation (ADEV) of the measurement corrected for the

tides and local environmental effects is shown in Fig. 2 (b), indicating a short-term stability of 13×10^{-8} m.s^{-2} at 1 s and a long-term stability of 2 nm.s^{-2} in 3 hours. This is about 10 times above the calculated QPN limit (dash-dotted line), as a result of the uncorrelated vibration noise. In a vibrationally more stable environment, a best short-term stability of 5.7×10^{-8} m.s^{-2} at 1 s was demonstrated [20]. The accuracy of CAG is 4.3×10^{-8} m.s^{-2} [21], mainly limited by the bias caused by the wave-front aberration of the Raman lasers.

We have also applied the same isolation and correlation techniques to the LNE-SYRTE gyroscope, which uses cesium-133 atoms in a fountain configuration and realizes a four-pulse interferometer. The general idea was first discussed in [22], and the experimental setup was described in [23]. Here, two mechanical accelerometers are used to record the vibration of the experimental structure. A weighted sum of these signals yields the vibration noise Φ_{vib} at the center of the interferometer. Given the large interrogation time of up to 800 ms and a corresponding macroscopic Sagnac area of 11 cm^2, Φ_{vib} is often beyond 20 rad peak-to-peak [see Fig. 3 (a)], rendering a linear correction impossible. Instead, we fit 20 data points to a sinusoid in order to obtain the rotation phase $\Phi_{\mathrm{sig}} = \Phi_\Omega$. This gives a vibration rejection efficiency of 6, as shown in Fig. 3 (b). We thus achieve a short-term stability of 160 nrad.s^{-1} at 1 s and a long-term stability of 4.4 nrad.s^{-1} after 1300 s.

We have seen that passive isolation and post correlation with classical sensors amount to apply a low pass filter that corrects the atomic sensor from higher-frequency vibration noise. In practice, the efficiency of this method is limited by the intrinsic noise and the nonlinearity of the classical sensor, and by the fact that the recorded vibration noise does not perfectly reproduce the vibration of the retroreflection mirror seen by the atoms. Nevertheless, atomic sensors such as CAG equipped with this system combine high performance and transportability, and can therefore perform precision measurements for metrology at different sites [4]. In particular, CAG has been participating in international comparisons of absolute gravimeters since 2009 [21, 24], and its measurements are in excellent agreement with those from other instruments.

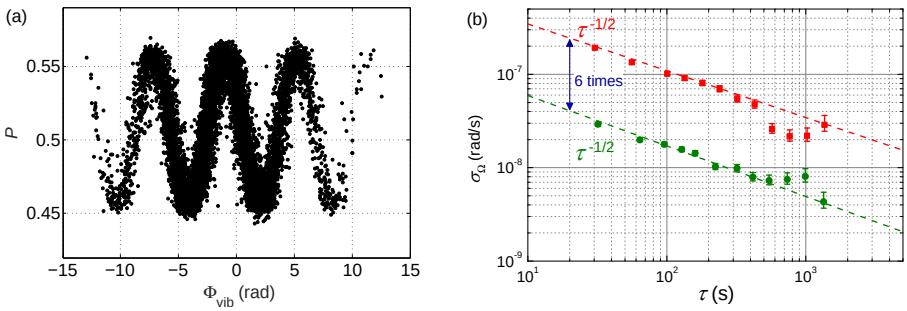

Figure 3. (a) Transition probability P vs the computed vibration phase Φ_{vib}. (b) ADEV of the measured rotation rate before (squares) and after (circles) correlation.

4. Vibration Compensation in Real Time and Hybridizing Atomic and Classical Sensors

Environmental stability is rarely guaranteed in field applications. Moreover, inertial navigation requires the sensors to follow the moving frame of the vehicle, hence necessitates the removal of any isolation [25, 6]. Such scenarios, together with the intrinsic high sensitivity of AI-based inertial sensors, result in the scatter of the data points beyond the linear regime, and thus a reduction of sensitivity. We demonstrate a procedure of compensating the vibration phase in real time, and the hybridization of an atomic and a classical accelerometers [26].

We operate a previous prototype of CAG [14, 27] in Paris city. The vibration signal is acquired using a mechanical accelerometer rigidly fixed to the experimental frame. A field programmable gate array (FPGA) based calculator treats the digitized acceleration signal to estimate the vibration phase Φ_{vib}. About 400 μs before the final interrogation pulse, the FPGA commands a phase jump in the direct digital synthesizer (DDS) that controls the phase lock of the Raman lasers. Such a feed forward scheme [see Fig. 4 (a)] allows us to operate the atomic sensor at mid fringe with little scatter. The vibration rejection efficiency can be as high as 60.

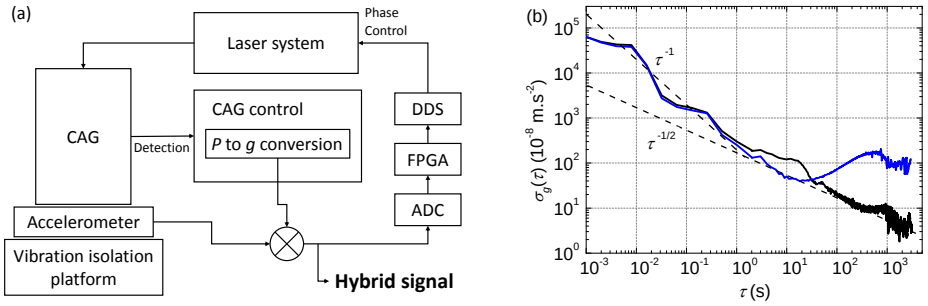

Figure 4. (a) Illustration of the real-time-compensation scheme and the hybridization with classical sensors. (b) ADEV of a classical accelerometer (blue) and a hybrid gravimeter (black). (b) is originally published in [26].

Further more, we perform a hybridization of the accelerometer with CAG. The DC component of conventional accelerometers suffers from drift and temperature dependence that severely degrades the long-term stability of the acceleration measurement. By locking the DC component on the CAG output, we realize a hybrid sensor which combines the large bandwidth (DC to 430 Hz) of the accelerometer and the bias stability and the accuracy of CAG. We show in Fig. 4 (b) the ADEV of the hybrid sensor placed on a vibration isolation platform. The short-term stability of the sensor is determined by the self-noise of the accelerometer and vibrations. The ADEV decreases as τ^{-1}, as high-frequency vibrations are averaged without dead time by the accelerometer. The long-term stability decreases as $\tau^{-1/2}$, indicating that it is set by CAG operating in the sequential mode and limited by the quality of the correlation. The added value of this technique for inertial navigation is assessed in [26].

5. Eliminating Dead Time

We have seen that the long-term stability of a hybrid inertial sensor still suffers from the dead time of the AI operating in sequential mode, which prevents efficient averaging of low-frequency noise (typically due to vibration). We present here a demonstration of a continuous atom interferometer without dead time, which paves the way to the intrinsically limited performance of AI-based inertial sensors.

We operate the fountain gyroscope mentioned in Sec. 3 as an atomic clock [23], using a sequence of two Raman pulses ($\pi/2$-$\pi/2$) so that $\Delta\Phi = \phi_1 - \phi_2$. We add a white noise over a bandwidth of 400 Hz to the local oscillator (LO) which controls the phase lock of the two Raman lasers. The added noise is analogous to the vibration noise in atomic inertial sensors. The cycle time and the Ramsey time are matched to be 480 ms, and each Raman pulse is shared between two atom clouds, one leaving and the other entering the interrogation zone, as shown in Fig. 5 (a). This imprints the same LO noise on consecutive interferometric phases , i.e. $\phi_2^i = \phi_1^{i+1}$, allowing cancellation of the LO noise in the interferometric phase accumulated over multiple shots. As a result, the ADEV of the relative frequency stability of the continuous clock follows

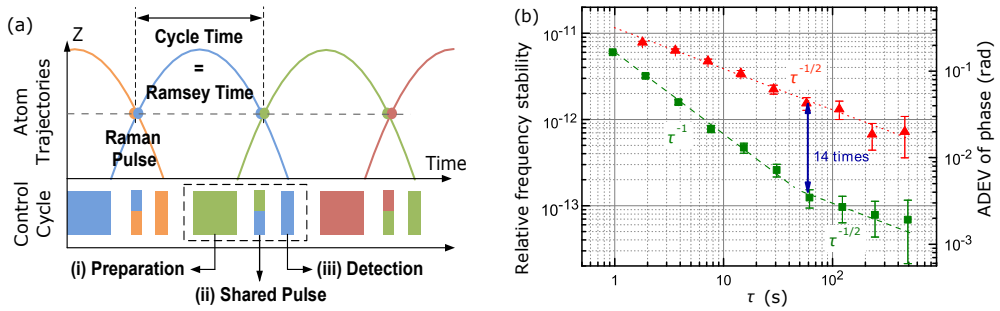

Figure 5. (a) Illustration of the zero-dead-time sequence of the atom gyroscope in the clock mode. (b) ADEV of the atomic clock in normal (triangles) and continuous (squares) mode. This figure is originally published in [23].

the τ^{-1} scaling, as shown in Figure 5 (b) (squares). The same figure shows the ADEV of a sequential clock (triangles), which follows the $\tau^{-1/2}$ scaling. The continuous clock gives a 14-fold gain in the relative frequency stability at 60 s. Thereafter, both are limited by uncorrelated noise (e.g. detection noise), and follow the $\tau^{-1/2}$ scaling. Note that the performance of the continuous clock after 60 s coincides with that of a sequential clock without the additional noise in the LO.

6. Conclusions

We have shown various steps towards exploring the full sensitivity of AI-based inertial sensors, which currently face the problems associated with the vibration noise, aliasing and the dead time between measurements. These problems would only become more severe when the sensors leave the environmentally stable laboratories for field applications. Moreover, the need to measure a fluctuating inertial signal (e.g. in navigation) renders active or passive isolation undesirable. Our efforts to correlate and hybridize atomic and mechanical sensors i) demonstrate AI-based inertial sensors with high sensitivity, ii) improve the dynamics beyond the linear regime, and iii) partially remove the dead time between successive interrogations. They represent a major step forward in reducing the size and the complexity of the sensors, making them suitable for on-board and field applications, and have stimulated the commercialization of atomic inertial sensors [28]. Such instruments now participate in gravity measurements, and have the potential to perform inertial navigations. The ability to fully eliminate the dead time will eventually lead to a new generation of QPN limited high-performance inertial sensors exploiting the full potential of atom interferometry.

Acknowledgments

The authors would like to thank the Institut Francilien pour la Recherche sur les Atomes Froids (IFRAF), the Agence Nationale pour la Recherche (ANR-9-BLAN-0026-01) in the framework of the MiniAtom collaboration, the Action Spécifique Gravitation Références Astronomie et Métrologie (GRAM), the Centre National d'Etudes Spatiales (CNES), the Délégation Générale pour l'Armement (DGA), the LABEX Cluster of Excellence FIRST-TF (ANR-10-LABX-48-01) within the Program "Investissements d'Avenir" operated by ANR, the city of Paris through the Emergence programme (project HSENS-MWGRAV), and the European Metrology Research Programme (EMRP) within the kNOW project for financial support. The EMRP was jointly funded by its participating countries within the European Association of National Metrology Institutes (EURAMET) and the European Union.

References

[1] Riehle F, Kisters Th, Witte A, Helmcke J and Bordé Ch J 1991 *Phys. Rev. Lett.* **67** 177
[2] Kasevich M and Chu S 1991 *Phys. Rev. Lett.* **67** 181
[3] Berman P R 1997 *Atom Interferometry* (San Diego: Academic Press)
[4] Farah T, Guerlin C, Landragin A, Bouyer P, Gaffet S, Pereira Dos Santos F and Merlet S 2014 *Gyroscopy and Navigation* **5** 266
[5] Hauth M, Freier C, Schkolnik V, Peters A, Wziontek H and Schilling M 2013 *Proc. Int. Sch. of Phys. "Enrico Fermi"* vol 188, ed Tino G M and Kasevich M A (Bologna: IOS Press) pp 557-86
[6] Geiger R, Ménoret V, Stern G, Zahzam N, Cheinet P, Battelier B, Villing A, Moron F, Lours M, Bidel Y, Bresson A, Landragin A and Bouyer P 2011 *Nat. Comm.* **2** 474
[7] Altschul B *et al* for the STE-QUEST collaboration 2015 *Adv. Space Res.* **50** 501-5
[8] Dimopoulos S, Graham P W, Hogan J M, Kasevich M A and Rajendran S 2008 *Phys. Rev.* D **78** 122002
[9] Geiger R, Amand L, Bertoldi A, Canuel B, Chaibi W, Danquigny C, Dutta I, Fang B, Gaffet S, Gillot P, Holleville D, Landragin A, Merzougui M, Riou I, Savoie D and Bouyer P 2015 *Proc. 50th Rencontres de Moriond: "100 years after GR"* 21-18 March 2015 La Thuile, Italy
[10] Yver-Leduc F, Cheinet P, Fils J, Clairon A, Dimarcq N, Holleville D, Bouyer P and Landragin A 2003 *J. Opt.* B*: Quantum Semiclas. Opt.* **5** S136-42
[11] Santarelli G *et al* 1998 *IEEE Trans. Ultrason. Ferroelectr. Freq. Control* **45** 887-94
[12] Peters A, Chung K Y and Chu S 2001 *Metrologia* **38** 25-61
[13] Hu Z, Sun B, Duan X, Zhou M, Chen L, Zhan S, Zhang Q and Luo J 2013 *Phys. Rev.* A **88** 043610
[14] Le Gouët J, Mehlstäubler T E, Kim J, Merlet S, Clairon A, Landragin A and Pereira Dos Santos F 2008 *Appl. Phys.* B **92** 133-44
[15] Jekeli C 2005 *Navigation* **52** 1-14
[16] Antoine Ch and Bordé Ch J 2003 *J. Opt.* B*: Quantum Semiclass. Opt.* **5** S199
[17] Louchet-Chauvet A, Farah T, Bodart Q, Clairon A, Landragin A, Merlet S and Pereira Dos Santos F 2011 *New J. Phys.* **13** 065025
[18] Cheinet P, Canuel B, Pereira Dos Santos F, Gauguet A, Leduc F and Landragin A 2008 *IEEE Trans. on Instrum. Meas.* **57** 1141
[19] Merlet S *et al* 2008 *Metrologia* **45** 26574
[20] Gillot P, Francis O, Landragin A, Pereira Dos Santos F and Merlet S 2014 *Metrologia* **51** L15-7
[21] Francis O *et al* 2013 *Metrologia* **50** 257-68
[22] Canuel B, Leduc F, Holleville D, Gauguet A, Fils J, Virdis A, Clairon A, Dimarcq N, Bordé Ch J, Landragin A and Bouyer P 2006 *Phys. Rev. Lett.* **97** 010402
[23] Meunier M, Dutta I, Geiger R, Guerlin C, Garrido Alzar C L and Landragin A 2014 *Phys. Rev.* A **90** 063633
[24] Jiang Z *et al* 2012 *Metrologia* **49** 666-84
[25] Merlet S, Le Gouët J, Bodart Q, Clairon A, Landragin A, Pereira Dos Santos F and Rouchon P 2009 *Metrologia* **46** 87-94
[26] Lautier J, Volodimer L, Hardin T, Merlet S, Lours M, Pereira Dos Santos F and Landragin A 2014 *Appl. Phys. Lett.* **105** 144102
[27] Merlet S, Volodimer L, Lours M and Pereira Dos Santos F 2014 *Appl. Phys.* B **117** 749
[28] Muquans Absolute Quantum Gravimeter http://www.muquans.com/index.php/products/aqg